Digital Discovery

ROYAL SOCIETY OF CHEMISTRY

PAPER

View Article Online
View Journal | View Issue

Cite this: *Digital Discovery*, 2026, **5**, 1228

Mapping Bloch-Redfield dynamics into a unitary gate-based quantum algorithm

Koray Aydoğan, [a] Maryam Abbasi,[b] Whitney J. Short,[c] Mikayla Z. Fahrenbruch,[b] Timothy J. Krogmeier, [b] Anthony W. Schlimgen [b] and Kade Head-Marsden *[b]

Recent progress in quantum computation has allowed for the simulation of dissipative quantum dynamics on current noisy quantum hardware. While most of these algorithms currently rely on phenomenological frameworks, microscopic approaches offer essential insights into various relaxation processes. Within classical simulation, the Bloch-Redfield equation serves as a microscopic method for modeling relaxation dynamics with applications in quantum information science and spintronics. Here, we utilize a diagonal dilation approach to map the Bloch-Redfield master equation in Liouville space into a compact set of circuits to simulate the dissipation of a spin system, akin to a dissipative process for a single molecule magnet. We demonstrate this algorithm in a variety of parameter regimes, including at different temperatures and external magnetic field strengths, on both quantum simulators and IonQ's Aria-1 quantum computer. This work broadens the scope of dissipative dynamics simulatable on quantum platforms.

Received 11th September 2025
Accepted 30th January 2026

DOI: 10.1039/d5dd00405e

rsc.li/digitaldiscovery

1. Introduction

In recent years, there has been remarkable development in quantum computing science, especially with respect to addressing challenges in computational chemistry.[1–3] While hardware, software, and error correction have all improved, we remain in the Noisy-Intermediate Scale Quantum (NISQ) era where we have access to relatively few qubits, that are highly susceptible to noise.[4,5] In this regime, hybrid quantum-classical approaches have shown great promise by leveraging both classical and quantum computers for their respective strengths.[6] Early use of hybrid quantum-classical algorithms in chemical applications focused primarily on the static electronic structure problem, with a heavy emphasis on Variational Quantum Eigensolvers to find ground state energies of molecular systems.[7–9] More recently, applications of these algorithms have expanded to advance computational catalysis,[10,11] drug design and metabolism,[12–15] and modeling of dissipative, or open, quantum system dynamics.[16,17]

Regarding dissipative quantum systems, current simulations of non-unitary evolution are restricted by both typical algorithmic challenges and the unitary computing architecture of many available hardware platforms. To address the latter issue, several block-encoding quantum algorithms dilate the Hilbert space of the non-unitary system into a unitary framework *via* techniques such as the Sz-Nagy dilation, unitary dilation of diagonals, and unitary decomposition approaches.[18–27] Open quantum systems can also be modeled on quantum hardware with a variety of other methods, including purification,[28,29] quantum imaginary time evolution,[30–32] variational techniques,[33–38] collision models,[39–41] and Monte Carlo simulations,[42] among others.[43–54]

While the design of hybrid quantum-classical algorithms to capture dissipative dynamics in general is challenging, the majority of current research has focused on applying the Gorini–Kossakowski–Sudarshan–Lindblad (GKSL) formalism.[31,55–60] The GKSL equation is a phenomenological approach to modeling dissipative dynamics[61,62] which has been applied in both the zero- and finite-temperature limits.[45,63,64] While phenomenological approaches provide many benefits including ease of use, often a microscopic approach is desirable. Classically there are several microscopic open quantum system approaches to simulate temperature-dependent relaxation,[65–69] though these approaches may not preserve positivity throughout the time evolution.[70–72] The Bloch-Redfield formulation,[73,74] derived under the Born-Markov approximation, is effective for capturing steady-state populations and relaxation dynamics for a variety of chemical and molecular systems at temperature, notably in the fields of photosynthetic light harvesting[75–77] and single molecule magnets (SMMs).[76,78–81] In SMMs, for example, observed spin relaxation is mostly determined by the spin-phonon relaxation (T_1), which is highly temperature dependent.[82,83] The quantum simulation of the Bloch-Redfield equation on quantum hardware could facilitate

[a]*School of Physics and Astronomy, University of Minnesota, Minneapolis, MN 55455, USA*

[b]*Department of Chemistry, University of Minnesota, Minneapolis, MN 55455, USA. E-mail: khm@umn.edu*

[c]*Department of Chemistry, Washington University in St. Louis, St. Louis, MO 61630, USA*

the study of temperature-driven relaxation in open quantum systems, providing insight into the behavior and properties of molecules and advanced spin-devices at ambient temperatures.

Here, we introduce a hybrid quantum-classical algorithm to consider the dynamical evolution of a molecular spin system under the influence of a bosonic reservoir *via* an ohmic spectral density using the Bloch-Redfield equation. We demonstrate our algorithm by simulating the dynamics of a two-level system interacting with an external magnetic fied, which is the simplest model of an SMM. By determining the form of the quantum circuits directly with respect to the system and environment parameters, our Redfield-based quantum algorithm is general for treating molecular spin relaxation under different system-environment coupling parameters. The present form of this algorithm is not designed with fault-tolerant quantum computing in mind; instead this approach presents a NISQ-friendly algorithm with compact circuits, demonstrated on both noisy quantum simulators and IonQ's Aria-1 quantum machine. Importantly, this work broadens the scope of simulatable dissipative dynamics on quantum hardware to a regime where a spectral function can be explicitly included into the circuit parameters.

2. Theory

2.1. Redfield equation

The Bloch-Redfield master equation is a microscopically-derived open systems approach to consider environmentally-driven dynamics under the Born-Markov approximation.[70,73,74,84] These approximations imply that this theory is valid for weak system-environment couplings, and when the environment relaxes sufficiently quickly such that memory effects do not play a role in the dynamics. The dynamics of a system's density matrix ρ can be written in atomic units as,

$$\frac{\mathrm{d}\rho}{\mathrm{d}t} = -i\left[\hat{H}, \rho\right] + \sum_{j,k}\left(-\hat{s}_j \hat{V}\hat{q}_{jk}\hat{V}^\dagger \rho + \hat{V}\hat{q}_{jk}\hat{V}^\dagger \rho \hat{s}_j - \rho \hat{V}\hat{q}'_{jk} V^\dagger \hat{s}_j + \hat{s}_j \rho \hat{V}\hat{q}'_{jk}\hat{V}^\dagger \right), \tag{1}$$

where $\hat{H}$ is the system Hamiltonian, $\hat{V}$ are the eigenvectors of $\hat{H}$, and $\hat{s}_j$ are the system operators which dictate how the system couples to an environment.[76,85] The strength of coupling to the environment is represented through the $\hat{q}$ operators as,

$$\left(\hat{q}_{jk}\right)_{n,m} = \frac{1}{2} C_{jk}(\omega_m - \omega_n)\left(\hat{V}^\dagger \hat{s}_k \hat{V}\right)_{n,m}, \tag{2}$$

and

$$\left(\hat{q}'_{jk}\right)_{n,m} = \frac{1}{2} C_{kj}(\omega_n - \omega_m)\left(\hat{V}^\dagger \hat{s}_k \hat{V}\right)_{n,m}, \tag{3}$$

where ω are the eigenvalues of $\hat{H}$, n, m denote the matrix elements with respect to a basis indexed with n and m,[76] and C_{jk} is the spectral function, which describes the temperature-dependent distribution of coupling frequencies present in the environment. This equation can also be written as a propagator equation in the so-called Liouville space,[86]

$$|\rho(t)\rangle = e^{\mathcal{R}t}|\rho(t_0)\rangle, \tag{4}$$

where

$$\begin{aligned}\mathcal{R} = {} & i(\hat{H}^T \otimes \mathbb{1} - \mathbb{1} \otimes \hat{H}) \\ & + \sum_{j,k}(-\mathbb{1} \otimes \hat{s}_j \hat{V}\hat{q}_{jk}\hat{V}^\dagger + \hat{s}_j^T \otimes \hat{V}\hat{q}_{jk}\hat{V}^\dagger) \\ & - \sum_{j,k}(\hat{s}_j^T \hat{V}^* \hat{q}'^T_{jk}\hat{V}^T \otimes \mathbb{1} - \hat{V}^* \hat{q}'^T_{jk}\hat{V}^T \otimes \hat{s}_j),\end{aligned} \tag{5}$$

where $\mathbb{1}$ is the identity operator, and $\otimes$ is the Kronecker product. The dimension of the vectorized density matrix, $|\rho(t)\rangle$, is quadratically larger than the dimension of ρ in the original Hilbert space; however, $|\rho(t)\rangle$ can be normalized to be a pure state in Liouville space, which facilitates the simulation of the dynamics on unitary quantum computers.

2.2. Unitary mapping of Bloch-Redfield dynamics

The propagator in eqn (4) is in general non-unitary, which requires a unitary mapping for implementation on unitary-gate-based quantum devices. We use a diagonal dilation technique to apply the exponentiated superoperator probabilistically.[21,60] This requires diagonalizing the propagator; however, we find this yields a parameterized quantum circuit for the propagation with respect to the system-environment variables and time. This circuit is generally applicable to any two-level system evolving according to the Bloch-Redfield equation, thus the cost of diagonalization produces a parameterized quantum circuit that can simulate a variety of dynamical evolutions. The superoperator in eqn (5) is diagonalizable under appropriate parameter regimes,

$$\mathcal{R}_\mathrm{d} = K^{-1}\mathcal{R}K, \tag{6}$$

where K is an invertible transformation matrix, or the matrix of eigenvectors, and $\mathcal{R}_d$ is the diagonalized Bloch-Redfield tensor. The dynamical evolution in the vectorized equation can then be written as,

$$\begin{aligned}|\rho(t)\rangle &= Ke^{\mathcal{R}_\mathrm{d}t}K^{-1}|\rho(0)\rangle \\ &= Ke^{\mathcal{R}_\mathrm{d}t}|\tilde{\rho}(0)\rangle,\end{aligned} \tag{7}$$

where $|\tilde{\rho}(0)\rangle$ is the initial vectorized density matrix transformed with the transformation matrix K^{-1}. We then simulate $e^{\mathcal{R}_\mathrm{d}t}|\tilde{\rho}(0)\rangle$ *via* quantum gates, where we can use dilation techniques to apply the non-unitary diagonal operator $e^{\mathcal{R}_\mathrm{d}t}$.[21,87] This is in contrast to quantum trajectory approaches, where the density matrix is constructed by trajectory sampling. In that case, the system operators are in Hilbert space and the quantum jumps can be applied using ancilla resets. The complexity of the density matrix construction is sensitive to the system relaxation time, in constrast to direct superoperator methods like the vectorized approach described here. Through a minimal one-dilation, the dynamics can be simulated probabilistically, conditioned on the state of the single additional ancilla.

Specifically, a non-unitary diagonal matrix can be dilated into a unitary diagonal matrix,

$$e^{\mathcal{R}_d t} \rightarrow e^{\tilde{\mathcal{R}}_d t} = \begin{bmatrix} X_+ & 0 \\ 0 & X_- \end{bmatrix}, \tag{8}$$

where $X_\pm$ are diagonal matrices whose entries are,

$$X_{\pm,ii} = x_i \pm i x_i \sqrt{\frac{1 - \|x_i\|^2}{\|x_i\|^2}}, \tag{9}$$

where x_i are diagonal elements of $e^{\mathcal{R}_d t}$. Importantly $e^{\tilde{\mathcal{R}}_d t}$ and $X_\pm$ are unitary, and $X_+ + X_- = 2e^{\mathcal{R}_d t}$, which allows the use of the Linear Combination of Unitaries (LCU) technique to prepare the desired state probabilistically.[21,88] In general for an r-dimensional operator $\mathcal{R}_d$, the dilated unitary is $2r$, with the pairs $x_\pm$ on the diagonal. The circuit decompositions of diagonal unitaries have a well known form, which we use in the present work.[87] Exact implementation of diagonal operators scales exponentially; however, these operators can alternatively be implemented polynomially with controlled error.[89] The dilated operator is applied to a quantum state, and the positive linear combination of the subspaces results in the desired time evolution.

After measurement, the density matrix can be classically transformed to the original basis to obtain the system evolution. This classical transformation step results in the hybrid quantum-classical algorithm for simulating the Redfield dynamics. For quantum devices with reduced noise, we could apply both K^{-1} and K on the quantum circuit with additional ancilla qubits; however, the initial diagonalization of the Redfield superoperator is still performed classically. To measure observables of the dynamical system using a noisy quantum simulator, we apply K after the time-propagation.

2.3. Measuring observables

In addition to investigating the dynamics, this framework can be used to determine observables. To measure an observable of $\hat{O}$ on the quantum device directly, we must apply the transformation K on the device since, in general, K and $\hat{O}$ do not commute. The expectation value of a general observable can then be found through the Hadamard test.[90] We implement the non-unitary transformation matrix K on a quantum circuit by using the singular value decomposition (SVD),

$$K = U\Sigma P^\dagger, \tag{10}$$

where U and P are unitary matrices and Σ is diagonal and non-unitary.[21] In order to implement this decomposition, we dilate Σ to make it unitary using the same technique as in the previous section, requiring a second ancilla qubit.

3. Methods

The Bloch-Redfield equation yields an approximate method to consider processes such as excitonic transport through photosynthetic light-harvesting antennae,[75–77] electron-transfer dynamics,[91] and molecular spin relaxation in SMMs.[92,93] SMMs consist of transition metal ions coordinated to organic ligands with a paramagnetic electron housed on the ion. Techniques in synthetic chemistry offer a significant degree of flexibility in tuning the surrounding ligand field, making these systems relevant for contemporary technologies;[94–99] however, the vibrational structure of the SMMs limits their practical use *via* spin-phonon coupling induced relaxation at elevated temperatures.[100] As an example of our theory above, we will consider a two-level system coupled to a bosonic reservoir *via* an ohmic spectral density as the simplest example of an SMM starting with a specific coupling parameter, then generalize to arbitrary system-environment coupling.

The circuits derived in this section are analytically dependent on the system and environment parameters of the physical system being studied. This implies that the circuits derived in Section 3.1 can be used for any two-level system coupled to an environment with any spectral density through a $\hat{\sigma}_x$ interaction, including varying magnetic fields and temperatures. The parameters derived in Section 3.3 generalize further, lifting the constraint on the system-environment coupling operator, thus providing circuits parametrized for the most general two-level system Redfield dynamics.

3.1. Dynamics of a two-level system interacting with a bosonic reservoir

Consider an $S = \frac{1}{2}$ two-level system defined by the Hamiltonian,

$$\hat{H} = -\frac{\varepsilon}{2}\hat{\sigma}_z \tag{11}$$

where $\varepsilon = \mu_B B_0 g S$ is the Zeeman splitting energy in an external magnetic field B_0, μ_B is the Bohr magneton, g is the Landè tensor,[92] and $\hat{\sigma}_z$ is the Pauli-z operator. For this example, we will consider a system-coupling operator of the form $\hat{s} = \hat{\sigma}_x$, where $\hat{\sigma}_x$ is the Pauli-x operator. The environment will be a bath of phonons with a temperature-dependent population of modes, and we will invoke an ohmic spectral density to quantify the coupling strength between system and bath operators at each frequency,[76,101]

$$C_{jk}(\omega) = \omega \coth\frac{\hbar\omega}{2k_B T}\delta_{jk}, \tag{12}$$

with

$$C_{jk}(-\omega) = e^{\frac{-\hbar\omega}{k_B T}} C_{jk}(\omega), \tag{13}$$

where $\omega > 0$, δ_{jk} is the Kronecker delta function, k_B is the Boltzmann constant, $\hbar$ is reduced Planck's constant, and T is the temperature. This form is commonly used in the study of quantum optics and non-equilibrium statistical physics, where the thermal effects play a significant role in the dynamics.[76,101,102]

For a two-level system, the dimension of the propagator in Liouville space is 4, making the dilated unitary an 8 by 8, or 3-qubit, operator. For a 3-qubit diagonal unitary, we can apply the dilated $e^{\mathcal{R}_d t}$ to a quantum circuit with angles that are related to

the system and bath parameters of the dissipative two-level system. From the system Hamiltonian and the system-environment coupling operator $\hat{\sigma}_x$, we can rewrite $\mathcal{R}$ as,

$$\mathcal{R} = \mathcal{Q}^* \otimes \mathbb{1} + \mathbb{1} \otimes \mathcal{Q} + (\hat{\sigma}_x \otimes \hat{q} + \hat{q} \otimes \hat{\sigma}_x), \tag{14}$$

where

$$\mathcal{Q} = \left(-\frac{i}{2}\varepsilon\hat{\sigma}_z - \hat{\sigma}_x\hat{q} \right), \tag{15}$$

and

$$\hat{q} = \begin{bmatrix} 0 & \frac{1}{2}C(\omega_2 - \omega_1) \\ \frac{1}{2}C(\omega_1 - \omega_2) & 0 \end{bmatrix}. \tag{16}$$

Setting $a = \frac{1}{2}C(\omega_2 - \omega_1)$ and $b = \frac{1}{2}C(\omega_1 - \omega_2)$, the explicit form of $\mathcal{R}$ is given by,

$$\mathcal{R} = \begin{bmatrix} -2b & 0 & 0 & 2a \\ 0 & -a - b + i\varepsilon & a + b & 0 \\ 0 & a + b & -a - b - i\varepsilon & 0 \\ 2b & 0 & 0 & -2a \end{bmatrix}. \tag{17}$$

Under these conditions the transformation matrix and diagonal superoperator are written in terms of the dynamical parameters,

$$K = \begin{bmatrix} \frac{a}{b} & -1 & 0 & 0 \\ 0 & 0 & \frac{i\varepsilon - c}{a + b} & \frac{i\varepsilon + c}{a + b} \\ 0 & 0 & 1 & 1 \\ 1 & 1 & 0 & 0 \end{bmatrix}, \tag{18}$$

and,

$$\mathcal{R}_\mathrm{d} = \begin{bmatrix} 0 & 0 & 0 & 0 \\ 0 & -2a - 2b & 0 & 0 \\ 0 & 0 & -a - b - c & 0 \\ 0 & 0 & 0 & -a - b + c \end{bmatrix}, \tag{19}$$

where $c = \sqrt{(a + b - \varepsilon)(a + b + \varepsilon)}$. We note that K is non-invertible when $a + b = \varepsilon$.

After initial state preparation, we apply the diagonal dilated unitary $e^{\tilde{\mathcal{R}}_\mathrm{d} t}$ as a 3-qubit operator in terms of R_z and CNOT gates by using Walsh functions,[87]

$$e^{\tilde{\mathcal{R}}_\mathrm{d} t} = \prod_{j=1}^{N} e^{i a_j \hat{w}_j} \tag{20}$$

$$= R_z(\alpha_1) \oplus R_z(\alpha_2) \oplus R_z(\alpha_3) \oplus R_z(\alpha_4), \tag{21}$$

where N is the size of the dilated unitary, a_j are the Walsh coefficients, $\hat{w}_j$ are the Walsh functions, $\oplus$ is the direct sum, and $R_z(\alpha)$ is the rotation about the z-axis. The angles are,

$$\begin{aligned} \theta_1 &= \frac{1}{4}(\alpha_1 + \alpha_2 + \alpha_3 + \alpha_4), \\ \theta_2 &= \frac{1}{4}(\alpha_1 + \alpha_2 - \alpha_3 - \alpha_4), \\ \theta_3 &= \frac{1}{4}(\alpha_1 - \alpha_2 + \alpha_3 - \alpha_4), \\ \theta_4 &= \frac{1}{4}(\alpha_1 - \alpha_2 - \alpha_3 + \alpha_4), \end{aligned} \tag{22}$$

where $\alpha_i = \arctan(X_{\pm,ii})$ and $X_{\pm,ii}$'s are given by eqn (9), which are found from the exponential of the diagonal elements of $\mathcal{R}_\mathrm{d}$ in eqn (19). This circuit is shown in Fig. 1, and the explicit forms of the angles in terms of system-environment parameters are given in the SI.

After propagation with the diagonal operator, we perform conditional quantum state tomography on the 2-qubit system, which we perform by measuring the state repeatedly in the complete Pauli basis. The measurement cost is $\mathcal{O}(4^N)$ for N system qubits, and the number of required measurements scale as $\mathcal{O}\left(\frac{4^N}{\delta^2}\right)$ with precision δ. Next, we classically apply K on the result of the tomography, which returns the density matrix to the original basis. It is known that quantum state tomography does not give positive semi-definite (PSD) density matrix in general, so as a final classical step, we project the result to the nearest PSD density operator through semi-definite programming.[103–106] Alternatively, one can perform linear inversion optimization to find the nearest PSD density operator.[107]

3.2. Magnetization of a two-level system interacting with a bosonic reservoir

We determine the magnetization, M, of our molecular system by calculating the expectation value of $\hat{\sigma}_z$,

$$M = \mathrm{Tr}(\rho\hat{\sigma}_z). \tag{23}$$

Because the quantum state is in the Z-basis, we can compute magnetization directly from the populations of the ground- and excited-states after transformation by K, which requires neither full tomography nor the Hadamard test. To implement the non-unitary transformation K, we use the SVD-dilation method to make Σ unitary as we did for $e^{\mathcal{R}_\mathrm{d} t}$, previously shown in eqn (10) and (8). Notably, for the present example the SVD can be found analytically. With the SVD and the dilation on Σ, we implement

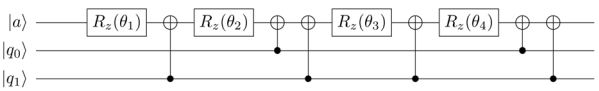

Fig. 1 Quantum circuit for the unitary dilated propagator $e^{\tilde{\mathcal{R}}_\mathrm{d} t}$. An ancillary qubit, $|a\rangle$, is introduced due to the dilation, and the angles are defined in the main text.

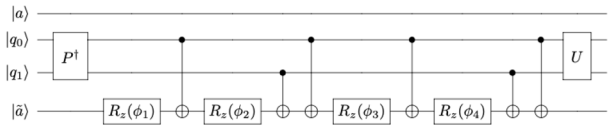

Fig. 2 Quantum circuit for the operator K, where $|a\rangle$ is the same ancilla for $e^{\bar{\mathcal{R}}_{\alpha}t}$, $|\tilde{a}\rangle$ is the second ancilla for K due to the dilation of Σ, and H is the Hadamard gate.

this decomposition on the circuit as shown in Fig. 2, where the angles ϕ_i's are derived in the same way for the angles θ_i's, and the $P^\dagger$ and U gates are the unitary matrices found from the SVD.

3.3. Extension to arbitrary system-environment couplings

In the circuits derived above the spectral density and external magnetic field are parameters that can be altered without the need for further derivations. To generalize this approach further, we can generalize the system-environment coupling operator beyond the $\hat{\sigma}_x$ chosen above. We can follow a similar procedure for a general system-environment coupling operator,

$$\hat{s} = \chi\hat{\sigma}_x + \beta\hat{\sigma}_y + \gamma\hat{\sigma}_z + \delta\mathbb{1} \tag{24}$$

where χ, β, γ, and δ are arbitrary constants and $\hat{\sigma}_i$ are Pauli gates. For simplicity we can define

$$a = \frac{1}{2}C(\omega_2 - \omega_1) \tag{25}$$

$$b = \frac{1}{2}C(\omega_1 - \omega_2) \tag{26}$$

$$d = \frac{1}{2}C(0), \tag{27}$$

in terms of an arbitrary spectral density. This allows the strength of the coupling to the environment to be encoded in the operators,

$$\hat{q} = \begin{bmatrix} d(\delta+\gamma) & a(\chi-i\beta) \\ b(\chi+i\beta) & d(\delta-\gamma) \end{bmatrix}. \tag{28}$$

We can also write $\mathcal{Q}$ and $\mathcal{R}$ with this coupling as,

$$\mathcal{Q} = i\hat{H} - \hat{s}^{\mathrm{T}}\hat{q}^* \tag{29}$$

$$\mathcal{R} = \mathcal{Q}\otimes\mathbb{1} + \mathbb{1}\otimes\mathcal{Q}^* + \hat{s}^T\otimes\hat{q} + \hat{q}^*\otimes\hat{s}. \tag{30}$$

Under these conditions, the transformation matrix and diagonal superoperator can also be found and therefore decomposed into a gate series where the arguments of the gates depend explicitly and analytically on the system-environment parameters outlined above. The full transformation matrix and diagonal operator are shown in the SI.

4. Results

We demonstrate this algorithm on two-level system dynamics under various temperatures and magnetic fields, simulating a variety of physical regimes. It should be noted that we focus on population dynamics and observables; however, we compute the full density matrix dynamics. Here, we use an initial state with no coherences, but given an initial state with non-zero coherence, this approach can also yield coherence dynamics. The ground- and excited-state population dynamics of a two-level system interacting with a bosonic reservoir *via* an ohmic spectral density at 25 K in a 1 T external magnetic field are shown in Fig. 3. Solid and dashed lines respectively represent the ground- and excited-state dynamics from classically solving the Redfield equation, and circles show results from IonQ's trapped ion Aria-1 device with 1000 shots. The Aria-1 device implements single-qubit gates *via* the native gate set, which consists of GPi, GPi2, and Virtual-Z gates by utilizing Rabi-oscillations made with a two-photon Raman transition,[108] while entangling operations are implemented *via* Mølmer–Sørensen gates.[109] Additional hardware specifications are given in the SI. After the circuit implementation on IonQ's Aria-1 is implemented with the debiasing error mitigation technique, the measurement statistics results are aggregated by a componentwise averaging strategy, introduced in ref. 110. Due to the compact circuits, the device data is in good agreement with the classical solution.

With the same circuit structure we consider these dynamics at varying temperatures shown in Fig. 4 with ground-state population as solid lines, excited-state populations as dashed lines, and results from 1024 shots on IonQ's simulator with the Aria-1 noise model as circles. As expected, as temperature increases, the relaxation times decrease.

We explore a range of external magnetic fields in Fig. 5 to demonstrate the effect of field strength on the dynamics. Again,

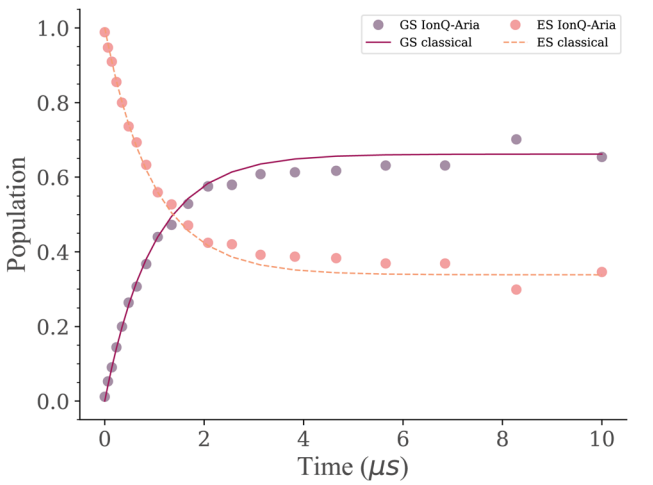

Fig. 3 Two-level system relaxation dynamics at 25 K in a 1 T external magnetic field due to interaction with an ohmic spectral density, where the classical ground (solid line) and excited (dashed line) populations and IonQ Aria-1 device data (circles) are shown.

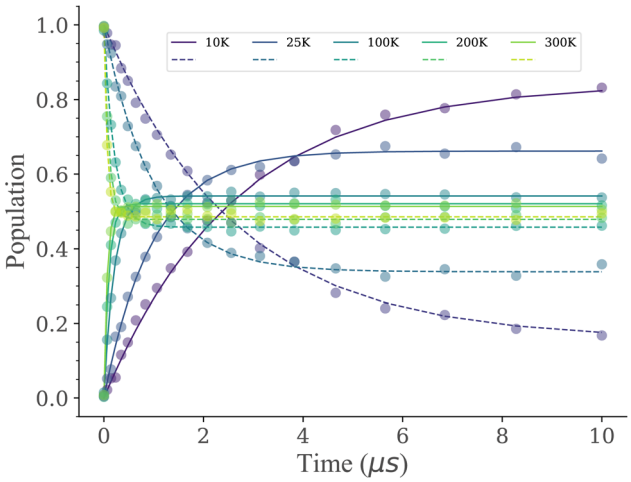

Fig. 4 Two-level system relaxation dynamics due to interaction with an ohmic spectral density in a 1 T external magnetic field, where the classical ground-state population (solid lines) and classical excited-state population (dashed lines) are shown at 10 K, 25 K, 100 K, 200 K, and 300 K, with results from IonQ's simulator with the Aria-1 noise model shown as circles for the ground and excited states.

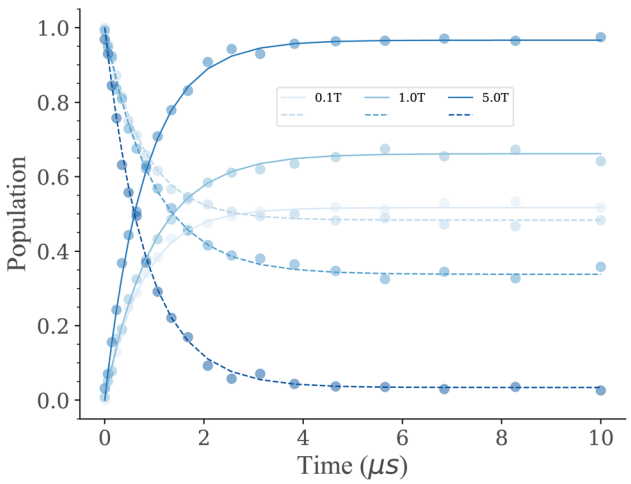

Fig. 5 Two-level system relaxation dynamics due to interaction with an ohmic spectral density at 25 K, where the classical ground-state population (solid lines), classical excited-state population (dashed lines), and IonQ simulator with the Aria-1 noise model results are shown at external magnetic fields of 0.1 T, 1 T, and 5 T.

solid and dashed lines respectively represent the ground- and excited-state dynamics from classically solving the Redfield equation, and circles the results from 1024 shots on IonQ's simulator with the Aria-1 noise model.

High magnetic fields lead to shorter T_1 time and higher magnetization for the spin system. In all of the regimes explored thus far, we can use the same circuit decomposition as demonstrated in Fig. 1, varying only the input angles based on temperature, external magnetic field, and time.

Finally, we calculate the expectation value of the system's magnetization *via* the circuit shown in Fig. 2. Fig. 6 shows the expectation value of the magnetization where the classical

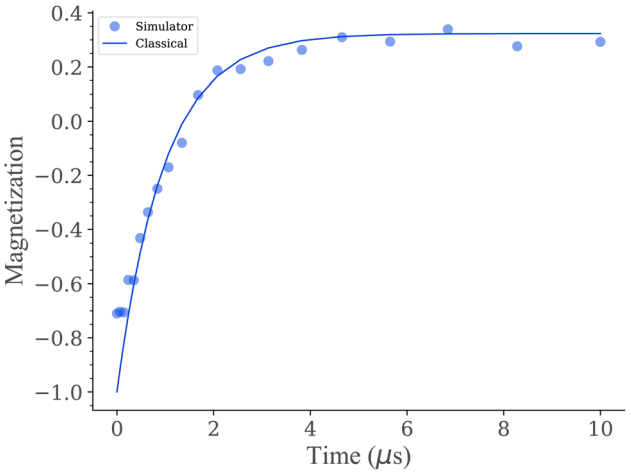

Fig. 6 Classical (line) and IonQ's simulator with the Aria-1 noise model (circles) expectation values of the magnetization of two-level system under 1 T external magnetic field at 25 K.

results are shown by a line, and the results from 1024 shots on IonQ's simulator with the Aria-1 noise model are shown as circles.

The simulator closely matches the classical result, and the magnetization becomes stable in the steady-state, as expected.

In all of these results, we show good agreement between the classical solution and either IonQ's Aria-1 device or IonQ's simulator with the Aria-1 noise model, with a relatively low number of required measurements. Since the system size is small, we perform full tomography; however, for larger systems, approaches like the Hadamard test or shadow tomography would be more appropriate.[90,111,112] While the cost of determining this circuit structure is relatively high, it allows for the derivation of a general circuit whose angle arguments depend directly on the original system parameters. This circuit needs to be derived only once to produce all of the data above, thus demonstrating the system and parameter scope attainable through a single diagonalization step.

5. Discussion and conclusions

We have mapped the Bloch-Redfield master equation into quantum algorithmic form to study the relaxation dynamics of a molecular spin system with an explicit spectral function, as a simple model of the dynamics and magnetization of an SMM. We derived circuits with parameters that depend explicitly on the molecular system, specifically on the Zeeman splitting, system-environment coupling, and spectral function of the environment. This requires explicit diagonalization of the Bloch-Redfield tensor to construct a time-independent similarity transformation into a diagonal basis. While this step is exponentially costly, it can be considered a classical pre-processing step to produce circuits that are general for the specific system-environment coupling chosen, in this case $\hat{s} = \hat{\sigma}_x$. This allows the same circuits to be used for any given time point, temperature, external magnetic field, Zeeman

splitting, and environmental spectral function. Moreover, these derived circuits are compact and therefore amenable to practical implementation on current quantum hardware, as demonstrated using IonQ's Aria-1 device.

An important contribution of this work is representing the propagation of the dilated Redfield operator in a fixed-form quantum circuit. In contrast, previous work required computing the SVD of the propagator at every time step,[60] whereas the present work provides a fixed and parameterized quantum circuit as a function of system-environment parameters and time, which can be used in future testing of Redfield dynamics of a two-level system. While this algorithm is developed for the current NISQ era, adaptations could be made in the future for fault-tolerant quantum computing. With improved devices, some of the classical overhead could be shifted to the quantum processors, such as diagonalization of the Redfield tensor by using quantum SVD or variational algorithms. While exact parameterization of a many-qubit system with this approach is intractable, the parameterization of the two-level system may still be useful in many-qubit settings. One potential application is molecular arrays where individual molecules are weakly coupled to one another. In this context this algorithm could be extended by perturbation theory with weak coupling approximations, using the circuit derived here. Moreover, future work could investigate applications of this algorithm to other systems, including more realistic single molecule magnets with multiple spins.

Conflicts of interest

There are no conflicts to declare.

Data availability

The data that supports the findings of this study are available in tables in the supplementary information (SI) of this article. Code, raw data, and scripts to generate figures are available through https://doi.org/10.5281/zenodo.17180822. Note that the data obtained from quantum noise models and hardware is accessed through tokens with IonQ. Results are statistical and new simulations could present small deviations from data generated in the manuscript. Supplementary information is available. See DOI: https://doi.org/10.1039/d5dd00405e.

Acknowledgements

KHM acknowledges partial support from the National Science Foundation through the University of Minnesota MRSEC under award Number DMR-2011401, along with start-up funding from the University of Minnesota. This research was supported by compute credits from IonQ *via* the QLab at the University of Maryland.

References

1 Y. Cao, J. Romero, J. P. Olson, M. Degroote, P. D. Johnson, M. Kieferová, I. D. Kivlichan, T. Menke, B. Peropadre, N. P. D. Sawaya, S. Sim, L. Veis and A. Aspuru-Guzik, *Chem. Rev.*, 2019, **119**, 10856.
2 P. Schleich, L. B. Kristensen, J. A. C. G. Angulo, D. Avagliano, M. Bagherimehrab, A. Aldossary, C. Gorgulla, J. Fitzsimons and A. Aspuru-Guzik, Chemically motivated simulation problems are efficiently solvable by a quantum computer, *Dig. Disc.*, 2026, **5**, 64–87.
3 R. Dutta, D. G. A. Cabral, N. Lyu, N. P. Vu, Y. Wang, B. Allen, X. Dan, R. G. Cortiñas, P. Khazaei, M. Schäfer, A. C. C. d. Albornoz, S. E. Smart, S. Nie, M. H. Devoret, D. A. Mazziotti, P. Narang, C. Wang, J. D. Whitfield, A. K. Wilson, H. P. Hendrickson, D. A. Lidar, F. Pérez-Bernal, L. F. Santos, S. Kais, E. Geva and V. S. Batista, *J. Chem. Theory Comput.*, 2024, **20**, 6426.
4 J. Preskill, *Quantum*, 2018, **2**, 79.
5 K. Bharti, A. Cervera-Lierta, T. H. Kyaw, T. Haug, S. Alperin-Lea, A. Anand, M. Degroote, H. Heimonen, J. S. Kottmann, T. Menke, W.-K. Mok, S. Sim, L.-C. Kwek and A. Aspuru-Guzik, *Rev. Mod. Phys.*, 2022, **94**, 015004.
6 A. Callison and N. Chancellor, *Phys. Rev. A*, 2022, **106**, 010101.
7 A. Peruzzo, J. McClean, P. Shadbolt, M.-H. Yung, X.-Q. Zhou, P. J. Love, A. Aspuru-Guzik and J. L. O'Brien, *Nat. Commun.*, 2014, **5**, 4213.
8 M. Cerezo, A. Arrasmith, R. Babbush, S. C. Benjamin, S. Endo, K. Fujii, J. R. McClean, K. Mitarai, X. Yuan, L. Cincio and P. J. Coles, *Nat. Rev. Phys.*, 2021, **3**, 625.
9 J. Tilly, H. Chen, S. Cao, D. Picozzi, K. Setia, Y. Li, E. Grant, L. Wossnig, I. Rungger, G. H. Booth and J. Tennyson, the Variational Quantum Eigensolver: a review of methods and best practices, *Phys. Rep.*, 2022, **986**, 1–128.
10 V. von Burg, G. H. Low, T. Häner, D. S. Steiger, M. Reiher, M. Roetteler and M. Troyer, *Phys. Rev. Res.*, 2021, **3**, 033055.
11 S. Hariharan, S. Kinge and L. Visscher, *J. Chem. Inf. Model.*, 2025, **65**, 472.
12 S. Yu, Z.-P. Zhong, Y. Fang, R. B. Patel, Q.-P. Li, W. Liu, Z. Li, L. Xu, S. Sagona-Stophel, E. Mer, S. E. Thomas, Y. Meng, Z.-P. Li, Y.-Z. Yang, Z.-A. Wang, N.-J. Guo, W.-H. Zhang, G. K. Tranmer, Y. Dong, Y.-T. Wang, J.-S. Tang, C.-F. Li, I. A. Walmsley and G.-C. Guo, *Nat. Comput. Sci.*, 2023, **3**, 839.
13 R. Santagati, A. Aspuru-Guzik, R. Babbush, M. Degroote, L. González, E. Kyoseva, N. Moll, M. Oppel, R. M. Parrish, N. C. Rubin, M. Streif, C. S. Tautermann, H. Weiss, N. Wiebe and C. Utschig-Utschig, *Nat. Phys.*, 2024, **20**, 549.
14 W. Li, Z. Yin, X. Li, D. Ma, S. Yi, Z. Zhang, C. Zou, K. Bu, M. Dai, J. Yue, Y. Chen, X. Zhang and S. Zhang, *Sci. Rep.*, 2024, **14**, 16942.
15 A. Caesura, C. L. Cortes, W. Pol, S. Sim, M. Steudtner, G.-L. R. Anselmetti, M. Degroote, N. Moll, R. Santagati, M. Streif and C. S. Tautermann, Faster quantum chemistry simulations on a quantum computer with improved tensor factorization and active volume compilation, *PRX Quantum*, 2025, **6**(3), 030337.
16 A. Miessen, P. J. Ollitrault, F. Tacchino and I. Tavernelli, *Nat. Comput. Sci.*, 2023, **3**, 25.

17 L. H. Delgado-Granados, T. J. Krogmeier, L. M. Sager-Smith, I. Avdic, Z. Hu, M. Sajjan, S. E. Abbasi, P. Narang, S. Kais, A. W. Schlimgen, K. Head-Marsden and D. A. Mazziotti, *Chem. Rev.*, 2025, **125**, 1823.
18 Z. Hu, R. Xia and S. Kais, *Sci. Rep.*, 2020, **10**, 3301.
19 K. Head-Marsden, S. Krastanov, D. A. Mazziotti and P. Narang, *Phys. Rev. Res.*, 2021, **3**, 013182.
20 A. W. Schlimgen, K. Head-Marsden, L. M. Sager, P. Narang and D. A. Mazziotti, *Phys. Rev. Lett.*, 2021, **127**, 270503.
21 A. W. Schlimgen, K. Head-Marsden, L. M. Sager-Smith, P. Narang and D. A. Mazziotti, *Phys. Rev. A*, 2022, **106**, 022414.
22 A. Gaikwad, Arvind and K. Dorai, *Phys. Rev. A*, 2022, **106**, 022424.
23 Z. Hu, K. Head-Marsden, D. A. Mazziotti, P. Narang and S. Kais, *Quantum*, 2022, **6**, 726.
24 N. Suri, J. Barreto, S. Hadfield, N. Wiebe, F. Wudarski and J. Marshall, *Quantum*, 2023, **7**, 1002.
25 Y. Wang, E. Mulvihill, Z. Hu, N. Lyu, S. Shivpuje, Y. Liu, M. B. Soley, E. Geva, V. S. Batista and S. Kais, *J. Chem. Theory Comput.*, 2023, **19**, 4851.
26 Y. Zhang, Z. Hu, Y. Wang and S. Kais, *J. Phys. Chem. Lett.*, 2023, **14**, 832.
27 D. Camps, L. Lin, R. Van Beeumen and C. Yang, *SIAM J. Matrix Anal. Appl.*, 2024, **45**, 801.
28 G. D. l. Cuevas, N. Schuch, D. Pérez-García and J. Ignacio Cirac, *New J. Phys.*, 2013, **15**, 123021.
29 L. H. Delgado-Granados, S. Warren, and D. A. Mazziotti, Unitary dynamics for open quantum systems with density-matrix purification, *arXiv*, 2024, preprint, arXiv:2406.01783, DOI: 10.48550/arXiv.2406.01783.
30 M. Motta, C. Sun, A. T. K. Tan, M. J. O'Rourke, E. Ye, A. J. Minnich, F. G. S. L. Brandão and G. K.-L. Chan, *Nat. Phys.*, 2020, **16**, 205.
31 H. Kamakari, S.-N. Sun, M. Motta and A. J. Minnich, *PRX Quantum*, 2022, **3**, 010320.
32 S.-H. Lin, R. Dilip, A. G. Green, A. Smith and F. Pollmann, *PRX Quantum*, 2021, **2**, 010342.
33 S. McArdle, T. Jones, S. Endo, Y. Li, S. C. Benjamin and X. Yuan, *npj Quantum Inf.*, 2019, **5**, 75.
34 M. Mahdian and H. D. Yeganeh, *J. Phys. Math. Theor.*, 2020, **53**, 13.
35 P. J. Ollitrault, S. Jandura, A. Miessen, I. Burghardt, R. Martinazzo, F. Tacchino and I. Tavernelli, *Quantum*, 2023, **7**, 1139.
36 S. Shivpuje, M. Sajjan, Y. Wang, Z. Hu and S. Kais, *Adv. Quantum Technol.*, 2025, **8**, 2400088.
37 T. M. Watad and N. H. Lindner, *Quantum Sci. Technol.*, 2024, **9**, 025015.
38 Z.-X. Shang, *Phys. Rev. A*, 2024, **109**, 062608.
39 K. Garg, Z. Ahmed, S. Mitra and S. Chakraborty, *Phys. Rev. A*, 2025, **112**, 022425.
40 L. K. Northcote, M. S. Teynor and G. C. Solomon, *J. Chem. Phys.*, 2025, **162**, 224112.
41 F. Gallina, M. Bruschi, R. Cacciari and B. Fresch, *J. Chem. Theory Comput.*, 2024, **20**, 10588.
42 G. Mazzola, *J. Chem. Phys.*, 2024, **160**, 010901.
43 B. Rost, L. Del Re, N. Earnest, A. F. Kemper, B. Jones, and J. K. Freericks, Demonstrating robust simulation of driven-dissipative problems on near-term quantum computers, *arXiv*, 2021, preprint, arXiv:2108.01183, DOI: 10.48550/arXiv.2108.01183.
44 P. Gupta and C. M. Chandrashekar, *New J. Phys.*, 2020, **22**, 123027.
45 F. Gallina, M. Bruschi and B. Fresch, *New J. Phys.*, 2022, **24**, 023039.
46 M. Cattaneo, M. A. C. Rossi, G. Garcia-Perez, R. Zambrini and S. Maniscalco, *PRX Quantum*, 2023, **4**, 010324.
47 L. Del Re, B. Rost, M. Foss-Feig, A. F. Kemper and J. K. Freericks, *Phys. Rev. Lett.*, 2024, **132**, 100601.
48 X. Li, S.-X. Lyu, Y. Wang, R.-X. Xu, X. Zheng and Y. Yan, *Phys. Rev. A*, 2024, **110**, 032620.
49 C. Long, L. Cao, L. Ge, Q.-X. Li, Y. Yan, R.-X. Xu, Y. Wang and X. Zheng, *J. Chem. Phys.*, 2024, **161**, 084105.
50 L. Hu and A. N. Jordan, *Phys. Rev. A*, 2024, **110**, 062205.
51 J. Peetz, S. E. Smart, S. Tserkis and P. Narang, *Phys. Rev. Res.*, 2024, **6**, 023263.
52 M. Bruschi, F. Gallina and B. Fresch, *J. Phys. Chem. Lett.*, 2024, **15**, 1484.
53 E. Borras and M. Marvian, *Phys. Rev. Res.*, 2025, **7**, 023076.
54 S. Chen, J. Chen and D. Davidović, *Phys. Rev. Appl.*, 2025, **24**, 034070.
55 R. Cleve and C. Wang, Efficient quantum algorithms for simulating lindblad evolution, *arXiv*, 2019, preprint, arXiv:1612.09512, DOI: 10.48550/arXiv.1612.09512.
56 H. Chen, N. Gomes, S. Niu and W. A. d. Jong, *Quantum*, 2024, **8**, 1252.
57 T. M. Watad and N. H. Lindner, *Quantum Sci. Technol.*, 2024, **9**, 025015.
58 J. Luo, K. Lin and X. Gao, *J. Phys. Chem. Lett.*, 2024, **15**, 3516.
59 A. W. Schlimgen, K. Head-Marsden, L. M. Sager, P. Narang and D. A. Mazziotti, *Phys. Rev. Res.*, 2022, **4**, 023216.
60 E. K. Oh, T. J. Krogmeier, A. W. Schlimgen and K. Head-Marsden, *ACS Phys. Chem. Au*, 2024, **4**, 393–399.
61 G. Lindblad, *Commun. Math. Phys.*, 1976, **48**, 119.
62 V. Gorini, A. Kossakowski and E. C. G. Sudarshan, *J. Math. Phys.*, 1976, **17**, 821.
63 B. Palmieri, D. Abramavicius and S. Mukamel, *J. Chem. Phys.*, 2009, **130**, 204512.
64 D. Manzano, *AIP Adv.*, 2020, **10**, 025106.
65 D. Tamascelli, A. Smirne, J. Lim, S. F. Huelga and M. B. Plenio, *Phys. Rev. Lett.*, 2019, **123**, 090402.
66 S. Davidson, A. Fruchtman, F. A. Pollock and E. M. Gauger, *J. Chem. Phys.*, 2020, **153**, 134701.
67 F. Nathan and M. S. Rudner, *Phys. Rev. B: Condens. Matter Mater. Phys.*, 2020, **102**, 115109.
68 A. Trushechkin, *Phys. Rev. A*, 2021, **103**, 062226.
69 S. Davidson, F. A. Pollock and E. Gauger, *PRX Quantum*, 2022, **3**, 020354.
70 H.-P. Breuer and F. Petruccione, *The Theory of Open Quantum Systems*, Oxford University Press, 2007.
71 A. Rivas and S. F. Huelga, *Open quantum systems*, Springer, 2012, vol. 10.

72 H. Weimer, A. Kshetrimayum and R. Orús, *Rev. Mod. Phys.*, 2021, **93**, 015008.
73 F. Bloch, *Phys. Rev.*, 1957, **105**, 1206.
74 A. G. Redfield, in *Advances in Magnetic and Optical Resonance*, Elsevier, 1965, vol. 1, pp. 1–32.
75 M. Richter, T. Renger and A. Knorr, *Photosynth. Res.*, 2008, **95**, 119.
76 J. Jeske, D. J. Ing, M. B. Plenio, S. F. Huelga and J. H. Cole, *J. Chem. Phys.*, 2015, **142**, 064104.
77 T. Uthailiang, O. Suntijitrungruang, P. Issarakul, P. Pongkitiwanichakul and S. Boonchui, *Sci. Rep.*, 2025, **15**, 5220.
78 A. Lunghi, *Sci. Adv.*, 2022, **8**, eabn7880.
79 A. Lunghi and S. Sanvito, *J. Chem. Phys.*, 2020, **153**, 174113.
80 M. Briganti, F. Santanni, L. Tesi, F. Totti, R. Sessoli and A. Lunghi, *J. Am. Chem. Soc.*, 2021, **143**, 13633.
81 J. Xu, A. Habib, S. Kumar, F. Wu, R. Sundararaman and Y. Ping, *Nat. Commun.*, 2020, **11**, 2780.
82 A. Lunghi and S. Sanvito, *J. Phys. Chem. Lett.*, 2020, **11**, 6273.
83 S. Takahashi, I. S. Tupitsyn, J. Van Tol, C. C. Beedle, D. N. Hendrickson and P. C. E. Stamp, *Nature*, 2011, **476**, 76.
84 F. Campaioli, J. H. Cole and H. Hapuarachchi, *PRX Quantum*, 2024, **5**(2), 020202.
85 J. Jeske and J. H. Cole, *Phys. Rev. A*, 2013, **87**, 052138.
86 T. F. Havel, *J. Math. Phys.*, 2003, **44**, 534.
87 V. Shende, S. Bullock and I. Markov, *IEEE Trans. Comput. Aided Des. Integrated Circ. Syst.*, 2006, **25**, 1000.
88 A. M. Childs and N. Wiebe, *Quant. Inf. Comput.*, 2012, **12**, 901–924.
89 J. Welch, D. Greenbaum, S. Mostame and A. Aspuru-Guzik, *New J. Phys.*, 2014, **16**, 033040.
90 M. A. Nielsen and I. L. Chuang, *Quantum Computation and Quantum Information: 10th Anniversary Edition*, Cambridge University Press, 2010.
91 J. M. Jean, R. A. Friesner and G. R. Fleming, *J. Chem. Phys.*, 1992, **96**, 5827.
92 A. Albino, S. Benci, L. Tesi, M. Atzori, R. Torre, S. Sanvito, R. Sessoli and A. Lunghi, *Inorg. Chem.*, 2019, **58**, 10260.
93 A. Lunghi, Spin-phonon relaxation in magnetic molecules: Theory, predictions and insights, in *Computational Modelling of Molecular Nanomagnets*, G. Rajaraman, Springer International Publishing, Cham, 2023, pp. 219–289.
94 L. Bogani and W. Wernsdorfer, *Nat. Mater.*, 2008, **7**, 179.
95 M. N. Leuenberger and D. Loss, *Nature*, 2001, **410**, 789.
96 Q. Yang, T. Zhong, Z. Tu, L. Zhu, M. Wu and X. C. Zeng, *Advanced Science*, 2019, **6**, 1801572.
97 L. Thomas, F. Lionti, R. Ballou, D. Gatteschi, R. Sessoli and B. Barbara, *Nature*, 1996, **383**, 145.
98 J. R. Friedman, M. P. Sarachik, J. Tejada and R. Ziolo, *Phys. Rev. Lett.*, 1996, **76**, 3830.
99 W. Wernsdorfer and R. Sessoli, *Science*, 1999, **284**, 133.
100 L. Escalera-Moreno, J. J. Baldoví, A. Gaita-Ariño and E. Coronado, *Chem. Sci.*, 2018, **9**, 3265.
101 A. J. Leggett, S. Chakravarty, A. T. Dorsey, M. P. A. Fisher, A. Garg and W. Zwerger, *Rev. Mod. Phys.*, 1987, **59**, 1.
102 J. H. Reina, L. Quiroga and N. F. Johnson, *Phys. Rev. A*, 2002, **65**, 032326.
103 B. Gärtner and J. Matousek, *Approximation algorithms and semidefinite programming*, Springer Science & Business Media, 2012.
104 S. Diamond and S. Boyd, *J. Mach. Learn. Res.*, 2016, **17**, 1.
105 A. Agrawal, R. Verschueren, S. Diamond and S. Boyd, *J. Control Decis.*, 2018, **5**, 42.
106 P. J. Goulart and Y. Chen, Clarabel: An interior-point solver for conic programs with quadratic objectives, *arXiv*, 2024, preprint, arXiv:2405.12762, DOI: 10.48550/arXiv.2405.12762.
107 J. A. Smolin, J. M. Gambetta and G. Smith, *Phys. Rev. Lett.*, 2012, **108**, 070502.
108 K. Wright, K. M. Beck, S. Debnath, J. M. Amini, Y. Nam, N. Grzesiak, J.-S. Chen, N. C. Pisenti, M. Chmielewski, C. Collins, K. M. Hudek, J. Mizrahi, J. D. Wong-Campos, S. Allen, J. Apisdorf, P. Solomon, M. Williams, A. M. Ducore, A. Blinov, S. M. Kreikemeier, V. Chaplin, M. Keesan, C. Monroe and J. Kim, *Nat. Commun.*, 2019, **10**, 5464.
109 K. Mølmer and A. Sørensen, *Phys. Rev. Lett.*, 1999, **82**, 1835.
110 A. Maksymov, J. Nguyen, Y. Nam, and I. Markov, Enhancing quantum computer performance *via* symmetrization, *arXiv*, 2023, arXiv: 2301.07233, https://arxiv.org/abs/2301.07233.
111 R. Cleve, A. Ekert, C. Macchiavello, and M. Mosca, *Proceedings of the Royal Society of London. Series A: Mathematical, Physical and Engineering Sciences*, 1969, vol. 454, pp. 339.
112 S. Aaronson, *SIAM J. Comput.*, 2020, **49**, STOC18.